Journal of Photonics for Energy

SPIEDigitalLibrary.org/jpe

Periodic nanostructuring for guided mode extraction in organic light-emitting diodes

Julian Hauss
Boris Riedel
Sebastian Gleiss
Ulf Geyer
Uli Lemmer
Martina Gerken

SPIE

Periodic nanostructuring for guided mode extraction in organic light-emitting diodes

Julian Hauss,[a,b] Boris Riedel,[a,b] Sebastian Gleiss,[a] Ulf Geyer,[b] Uli Lemmer,[a] and Martina Gerken[b]

[a] Light Technology Institute, Karlsruhe Institute of Technology (KIT), Kaiserstr. 12, D-76131 Karlsruhe, Germany

[b] Institute of Electrical and Information Engineering, Christian-Albrechts-Universität zu Kiel, Kaiserstr. 2, D-24143 Kiel, Germany

julian.hauss@kit.edu

Abstract. We investigated guided mode extraction in organic light-emitting diodes and compare the experimental findings to transfer matrix (T-matrix) and finite difference time domain (FDTD) simulations. To this end, we patterned the indium tin oxide anode with Bragg gratings with lattice constants from 300 to 600 nm and varied the depth of the grating structures. The structuring was done by laser interference lithography and plasma etching. Both techniques allow for a rapid large area processing. We measured angle resolved electroluminescent spectra of the nanostructured devices and reference devices. To obtain the mode distribution in the devices we made use of T-matrix simulations. In addition we performed FDTD simulations of the emission characteristics of the patterned devices. The simulations are in agreement with our experimental findings and give insight into the outcoupling mechanisms. [DOI: 10.1117/1.3544495]

Keywords: organic light-emitting diodes; light extraction; guided modes; transfer matrix; finite difference time domain; Bragg scattering.

Paper 10139SSPR received Aug. 15, 2010; revised manuscript received Dec. 17, 2010; accepted for publication Dec. 30, 2010; published online Feb. 3, 2011.

1 Introduction

Today, organic light-emitting diodes (OLEDs) are used in a variety of commercial display and lighting applications. They exhibit major advantages such as high power efficiency, Lambertian emission, and a wide color space, tunable by chemical synthesis of appropriate emitter molecules.[1,2] The internal quantum efficiency of OLEDs with phosphorescent emitters, harvesting also triplet excitons, can reach nearly 100%.[3,4] However, the external quantum efficiency of such devices is still limited by poor light extraction.[5–8] A common OLED consists of different thin organic layers, a transparent conductive anode layer, and a metallic cathode. The whole OLED thin film stack typically features an overall thickness of several hundred nanometers. Thus it resembles a planar waveguide structure in which the organic emission layer is part of the high index core. Hence, photon emission takes place inside a high index layer. This leads to the fact that about 50% of the emitted photons are emitted and trapped in guided modes in anode and organic layers and surface plasmon polaritons (SPPs) at the cathode/organic interface. Another 30% of the emitted photons are reflected at the substrate/air interface due to total internal reflection and only about 20% of the generated photons are able to leave the device as useful light if no further extraction techniques are applied.[9–11] In contrast to inorganic light-emitting diodes (LEDs), OLEDs are large area devices and thus the extraction techniques must be applicable on large areas. The extraction of light trapped in the substrate has been widely studied.[12] Typically

1947-7988/2011/$25.00 © 2011 SPIE

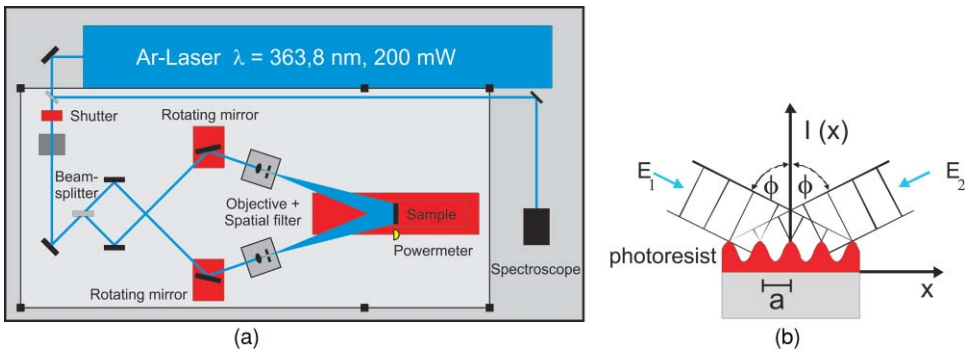

Fig. 1 (a) Laser interference lithography setup. The Ar^+ laser beam is split into two beams which are expanded and finally interfere at the sample position. (b) The interference pattern is used to expose a photoresist on top of the sample. In this way the interference pattern transfers into a photoresist grating. The grating period is determined by the angle of the two beams and the laser wavelength.

one modifies the back surface of the substrates. This process can be completely separated from the OLED fabrication. The extraction of the guided modes and surface plasmon polaritons is much harder to establish. The extraction elements must be close or even inside the OLED stack to have significant extraction efficiency for the guided modes and SPPs. Therefore micro- or even nanostructuring is required.[13–17]

Here we report periodic structuring of the indium tin oxide (ITO) anode layer of small molecule OLEDs. To fulfill the technology requirement of large area applicability we use laser interference lithography (LIL) and plasma etching for the nanostructure fabrication. The guided modes are extracted by coherent scattering at the grating structures (Bragg scattering). In Sec. 2 we briefly review the fabrication technology described in more detail in Ref. 15. Angle resolved emission spectrum measurements of the different devices are presented in Sec. 3. In Sec. 4 device simulations with the transfer matrix method (T-matrix) and the finite difference time domain (FDTD) method are presented and compared to the experimental results.

2 Device Fabrication

2.1 *Grating Fabrication by Laser Interference Lithography*

As a starting point for the grating fabrication we used standard prefabricated glass substrates with a 135 nm thick ITO layer. The ITO anode was structured by a combination of LIL and physical plasma etching, which allows for a rapid processing of large areas up to the square meter range.[18] The samples were coated with photoresist and subsequently exposed to a periodic light pattern formed by the superposition of two expanded beams of an Ar^+ laser with a wavelength of 363.8 nm (see Fig. 1).

The period of the interference pattern and thus the grating period are determined by the angle of the two beams and the laser wavelength. In this way we are able to tune the grating periodicity with our setup in the range of 300 up to 600 nm. Two-dimensional gratings can be obtained by a 90° sample rotation and a second exposure. After development of the resist we coated the samples with a chromium layer. Then, ultrasound assisted lift-off was used to transfer the grating into the chromium layer which was used subsequently as an etch mask for the physical plasma etching of the ITO. Argon plasma was used to etch the ITO layer. Via the etching time the grating depth could be set. Finally, the chromium was removed by wet etching.

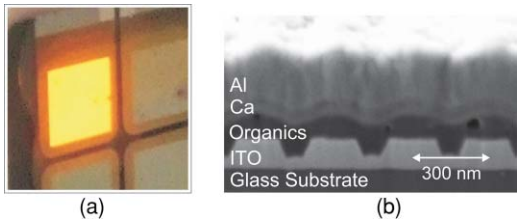

Fig. 2 (a) Photograph of a fabricated OLED. (b) Focused ion beam SEM image of an OLED with a structured ITO anode with a grating period of a = 300 nm.

2.2 *OLED Fabrication*

The fabrication of the OLEDs was done with standard evaporation processes. As an emitting layer we used tris-(8-hydroxyquinoline)aluminum (Alq_3) doped with 3% 4-(dicyanomethylene)-2-methyl-6-(4-dimethylaminostyryl)-4H-pyran (DCM), leading to a peak emission wavelength of about 600 nm. The following organic materials were deposited successively on the patterned substrates: a 50 nm thick *N*,*N*′-di (naphth-1-yl)-*N*,*N*′-diphenyl-benzidine (α-NPD) layer for hole transport, a 25 nm thick emission layer consisting of Alq_3 doped with 3% DCM, a 25 nm thick 2,9-dimethyl-4,7-diphenyl-1,10-phenanthroline (BCP) layer for hole blocking, followed by a 20 nm Alq_3 layer for electron transport. The metallic cathode consists of 50 nm Ca covered by a 250 nm thick Al layer. Finally the samples were encapsulated using an epoxy resin adhesive and a glass cover to allow for handling and measurements at normal atmospheric conditions. The active area of one device was 5 mm × 5 mm. Figure 2 shows a photograph of a fabricated OLED and an scanning electron microscope (SEM) image of a focused ion beam cut through an OLED with a 1D-grating with a period of 300 nm. The corrugation of the ITO-grating is transferred through all subsequent layers up to the Ca/Al electrode. Further details concerning the grating and OLED fabrication can be found in Ref. 15.

3 Electroluminescent Emission Measurements

We fabricated various devices with one-dimensional gratings with periods ranging from 600 nm down to 300 nm. We carried out angle resolved emission spectra measurements for the different OLEDs. The measurements were performed at room temperature using a source-measure unit (Keithley SMU 236), a spectrometer (Acton Research Corporation SpectraPro-300i) with an intensified charge-coupled device (ICCD) (Princeton Instruments PiMax:512), and a multimode fiber. The OLEDs emission spectra were recorded up to angles of $\theta = \pm 65^\circ$ in a plane perpendicular to the grating grooves. A scheme of the setup is given in Fig. 3.

Figures 4(a)–4(d) exemplarily show the spectral and angle resolved unpolarized emission of an unstructured reference OLED and three nanostructured OLEDs with grating periods of

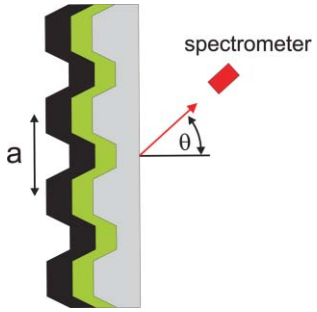

Fig. 3 Schematic measurement setup used for the angle resolved electroluminescent emission measurements.

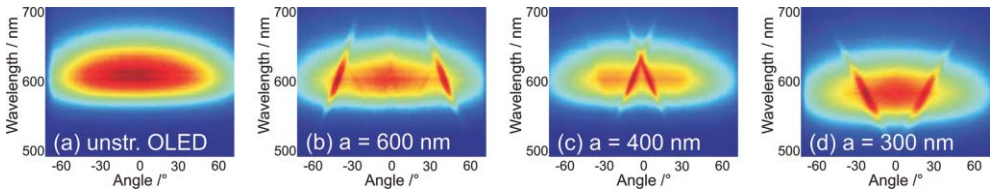

Fig. 4 Electroluminescent unpolarized emission of (a) an unstructured OLED and (b)–(d) OLEDs with ITO gratings with periods of 600, 400, and 300 nm.

600, 400, and 300 nm. The reference OLED exhibits a Lambertian-like emission, whereas the nanostructured OLEDs exhibit enhanced emission at certain angles due to outcoupling of guided modes. The angle of enhanced emission varies with wavelength and depends on the grating period chosen. A period of 400 nm leads to a more forward peaked mode extraction compared to other periods.

The wavelength and grating period dependence encountered can be explained by Bragg scattering of guided modes, $k_x' = k_x - m \cdot G$. Here, k_x and k_x' are the in-plane wave vector components perpendicular to the grating grooves before and after the scattering event and $G = 2\pi/a$ is the reciprocal lattice constant of the Bragg grating with period a. This leads directly to the following expression for the outcoupling angle of a certain mode:

$$\theta(a, \lambda_0) = \arcsin[\mathrm{Re}(n_{eff}) - m \cdot \lambda_0/a]. \tag{1}$$

Here a is the grating period, λ_0 is the vacuum wavelength, m is an integer number specifying the scattering order, and $n_{\mathrm{eff}} = k_x \cdot \lambda/(2\pi)$ is the effective index of refraction for a certain guided mode. To identify the polarization of the extracted modes a polarization filter was mounted in front of the multimode fiber guiding the light to the spectrometer. Figure 5(a) shows the angle resolved emission of an OLED with a 400 nm ITO grating at a wavelength of $\lambda = 600$ nm for TE and TM polarization. The TE-polarized emission is strongly peaked around $\theta = 6^\circ$ whereas in the TM-polarized emission no outcoupling peaks are encountered. Figure 5(b) shows the polarized emission spectra in normal direction to the device surface.

Furthermore, we built devices with different grating depths by making use of different etching times. These gratings had a period of 375 nm leading to outcoupling peaks in forward direction at a wavelength of $\lambda = 600$ nm. For this wavelength the angle resolved emission of devices with grating depths of 40 and 80 nm are given in Figs. 6(a) and 6(b). Figure 6(c) shows that the current-density voltage (J-V) characteristic of the devices is influenced by the grating depth. Therefore, in order to evaluate the extraction of the guided mode, the device emission is normalized by the emission at $\theta = 15^\circ$ where no outcoupling peaks are encountered.

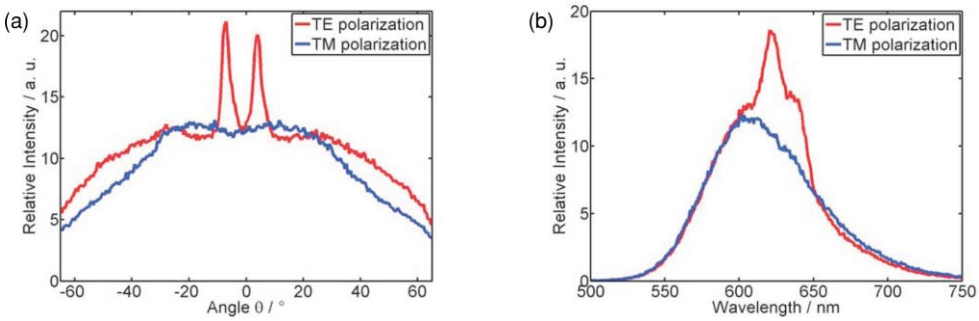

Fig. 5 TE-polarized (red) and TM-polarized (blue) electroluminescent emission of an OLED with an ITO grating with a period of $a = 400$ nm. (a) Angle resolved emission at the peak emission wavelength $\lambda = 600$ nm of the OLED. (b) Polarized emission spectra in normal direction to the device surface.

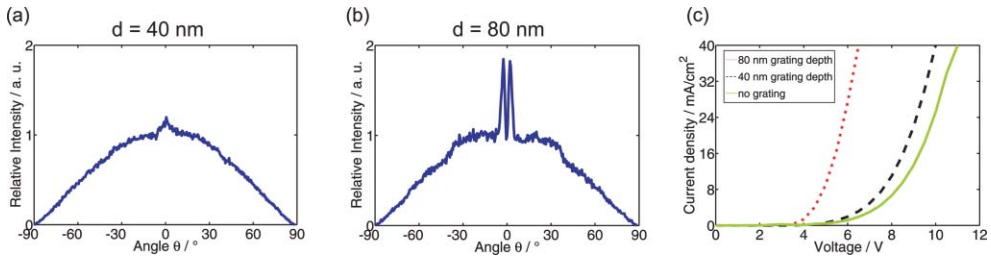

Fig. 6 Angle resolved emission of devices with grating depths of 40 nm (a) and 80 nm (b) at a wavelength of $\lambda = 600$ nm. Current-density voltage (J-V) characteristic (c) of devices with 40 nm grating depth (black dashed line) and 80 nm grating depth (red dotted line) compared to an unstructured reference device (green solid line).

The extraction efficiency increases with increasing grating depth. Furthermore, we see that the angular positions of the peaks slightly shift with increasing grating depth as the effective index of refraction of the outcoupled mode depends on the layer structure of the device and thus on the grating depth. It is important to note that an overall device optimization including optical and electrical properties might yield different layer thicknesses compared to an optimization of the flat device. On the other hand the gratings have to be deep and in turn efficient enough to compete with the modal absorption in the OLED stack.

4 Device Simulation

To identify the extracted modes and understand the basic principles of the extraction mechanism, we carried out T-matrix simulations. The simulations were done for an unstructured device with a reduced ITO layer thickness to account for the etching. To find guided modes we set the field at the metal interface to be purely exponentially decaying. Varying the real and imaginary part of the effective index of refraction n_{eff} (respectively the in-plane wave vector k_{x}) as free parameters we searched for solutions with a vanishing field in the glass substrate indicating an exponential decay at this side too. Figure 7 shows the result of such a parameter sweep for our OLED structure. It shows the electric field in the glass substrate as a function of the real and imaginary part of the effective index of refraction. In this plot, guided modes are found for values of n_{eff} associated with dips.

To get more precise results we used a two-dimensional minimum search algorithm around these dips. As a result we found two modes in the OLED waveguide structure, a TE_0 mode with

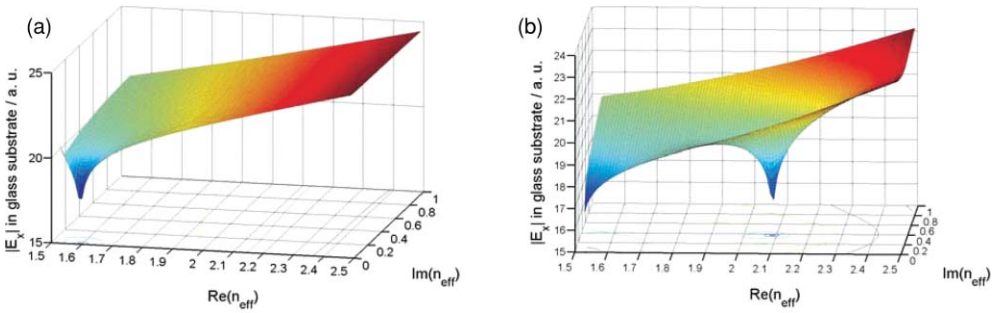

Fig. 7 Electric field in glass substrate as a function of real and imaginary part, of the effective index of refraction n_{eff}. (a) TE polarization. (b) TM polarization. In this plot, guided mode solutions are found for values of n_{eff} that are associated with dips, corresponding to a vanishing field in the glass substrate. For the TM case the high real and imaginary parts of the effective index of refraction indicate the surface plasmon polariton character of the mode.

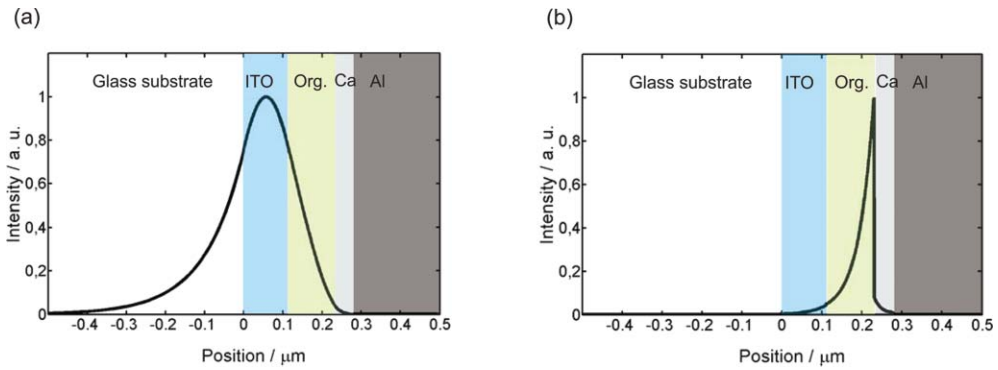

Fig. 8 Intensity profiles of the TE_0 mode (a) and TM_0/SPP mode (b) in the OLED structure for a vacuum wavelength of $\lambda = 600$ nm.

$n_{\text{eff}} = 1.6 + 0.004i$ and one SPP mode with $n_{\text{eff}} = 2.1 + 0.38i$. For the TM case the high real and imaginary parts of the effective index of refraction indicate the SPP character of the mode, in the following referred to as TM_0/SPP. For efficient outcoupling the mode must have a significant filling factor in the ITO layer where the grating is mainly located and the refractive index contrast to the subsequent organic layer is quite high. This is the case for the TE_0 in contrast to the TM_0/SPP mode as shown in the Figs. 8(a) and 8(b). The SPP mode decays exponentially toward the ITO anode and has no significant overlap with the grating region. Moreover, it is heavily damped due to the large imaginary part of the effective index of refraction.

Figures 9(a)–9(b) show the outcoupling angles calculated by T-matrix mode simulations and the Bragg scattering condition up to the second order according to Eq. (1) on top of the experimental data for OLEDs with different grating periods. From this comparison the significant outcoupling peaks can be associated with first order Bragg scattering of the TE_0 mode.

As an independent method for simulating the OLED emission characteristics we choose the FDTD method as OLEDs have a broad spectral emission and a time domain technique such as FDTD allows for a broadband simulation in just one run.[19] For our OLEDs with one-dimensional gratings we limited ourselves to two-dimensional simulations which reduce simulation time significantly compared to full three-dimensional simulations. The simulations were carried out with FDTD solutions from Lumerical. A line monitor slightly above the ITO

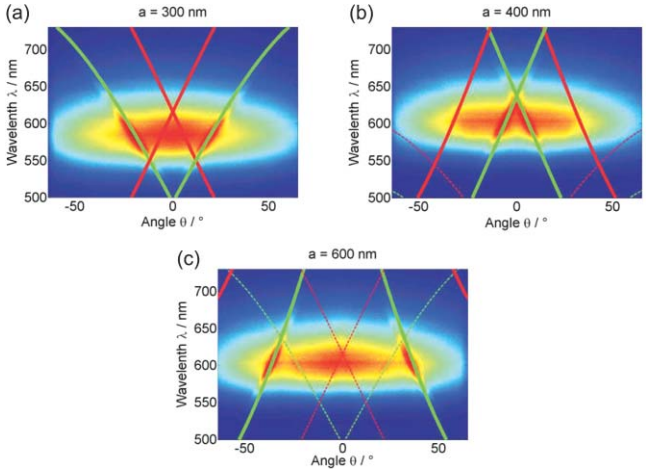

Fig. 9 Comparison of experimental data and calculated outcoupling angles for the TE_0 mode (green) and TM_0/SPP mode (red) based on T-matrix simulations and the Bragg scattering condition, according to Eq. (1). The bold lines indicate first order Bragg scattering ($m = 1$), the dashed lines second order Bragg scattering ($m = 2$).

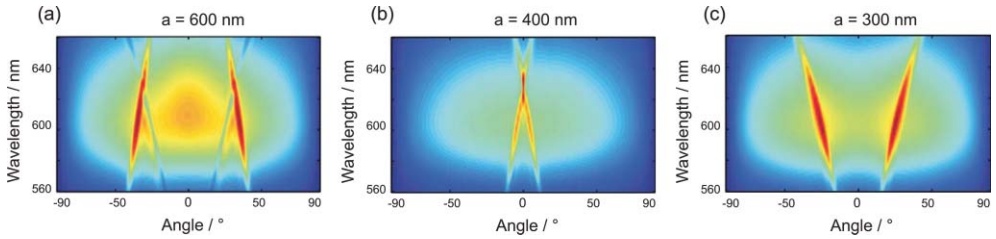

Fig. 10 FDTD calculations of angle resolved emission spectra of OLEDs with 300, 400, and 600 nm ITO gratings.

glass interface monitored the near-field emission from the device. Subsequently we used the near-to-far field projection algorithm of FDTD solutions to calculate the emission characteristics inside the glass substrate. Finally the device emission into air was obtained by application of the Fresnel relations for the glass air interface.

Evaporated small molecule emitters have no preferred orientation. To match this behavior with our simulation, we used three independent orthogonal dipole sources placed in each case at two different positions relative to the grating and summed up the far field intensities. The simulation area was surrounded by perfectly matched layer (PML) boundary conditions as reflections at the boundaries would lead to unphysical interference effects. The number of PMLs and the FDTD discretization were chosen such that a refinement of the discretization or additional PMLs would yield only a negligible change in the result. Figures 10(a)–10(b) show the emission of OLEDs with different ITO gratings as a function of the emission angle and wavelength.

A detailed comparison of the simulated and measured data reveals that the angular positions of the outcoupling peaks match perfectly. Furthermore, we performed simulations of the angle resolved emission of devices with a grating period of 375 nm and various grating depths. The results at a wavelength of $\lambda = 600$ nm are given in Fig. 11 and show analogously to the experiment that the outcoupling increases with grating depth and that the extraction angle varies slightly with increasing grating depth.

5 Conclusion

We fabricated OLEDs on nanostructured ITO anodes with enhanced guided mode extraction. The LIL we used allows for a smooth change of the grating period which allows for tuning of the outcoupling angle for mainly forward light extraction. T-matrix and FDTD simulations were in agreement with our experimental findings and enabled us to get insight into the mode extraction mechanisms. The latter method is suitable to simulate the influence of the grating geometry on the outcoupling efficiency as demonstrated exemplarily for the grating depth. To go beyond these optical simulations and to be able to analyze the effect of the gratings on

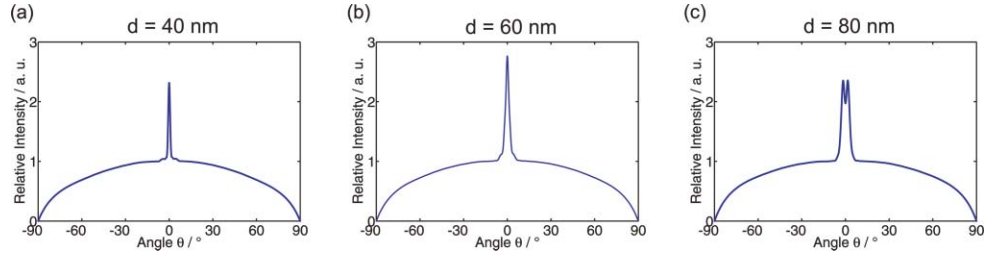

Fig. 11 FDTD simulations of the grating depth variation for devices with a grating period of 375 nm at a wavelength of $\lambda = 600$ nm.

the overall efficiency of OLEDs, three-dimensional FDTD simulations in combination with electrical simulations should be performed.

Acknowledgments

We acknowledge support by the Bundesministerium für Bildung und Forschung (BMBF) within the project NanoFutur (03X5514). J. Hauss and B. Riedel are pursuing their PhD within the Karlsruhe School of Optics & Photonics (KSOP).

References

1. S. R. Forrest, "The road to high efficiency organic light-emitting devices," *Org. Electron.* **4**, 45–48 (2003).
2. S. Reineke, F. Lindner, G. Schwartz, N. Seidler, K. Walzer, B. Lussem, and K. Leo, "White organic light-emitting diodes with fluorescent tube efficiency," *Nature (London)* **459**(7244), 234–238 (2009).
3. C. Adachi, M. A. Baldo, M. E. Thompson, and S. R. Forrest, "Nearly 100% internal phosphorescence efficiency in an organic light-emitting device," *J. Appl. Phys.* **90**(10), 5048–5051 (2001).
4. M. A. Baldo, D. F. O'Brien, Y. You, A. Shoustikov, S. Sibley, M. E. Thompson, and S. R. Forrest, "Highly efficient phosphorescent emission from organic electroluminescent devices," *Nature (London)* **395**(6698), 151–154 (1998).
5. N. K. Patel, S. Cina, and J. H. Burroughes, "High-efficiency organic light-emitting diodes," *IEEE J. Sel. Top. Quantum Electron.* **8**(2), 346–361 (2002).
6. N. C. Greenham, R. H. Friend, and D. D. C. Bradley, "Angular-dependence of the emission from a conjugated polymer light-emitting diode – implications for efficiency calculations," *Adv. Mater.* **6**(6), 491–494 (1994).
7. A. Chutinan, K. Ishihara, T. Asano, M. Fujita, and S. Noda, "Theoretical analysis on light-extraction efficiency of organic light-emitting diodes using fdtd and mode-expansion methods," *Org. Electron.* **6**(1), 3–9 (2005).
8. M. H. Lu and J. C. Sturm, "Optimization of external coupling and light emission in organic light-emitting devices: modeling and experiment," *J. Appl. Phys.* **91**(2), 595–604 (2002).
9. W. L. Barnes, "Electromagnetic crystals for surface plasmon polaritons and the extraction of light from emissive devices," *J. Lightwave Technol.* **17**(11), 2170–2182 (1999).
10. G. Gu, D. Z. Garbuzov, P. E. Burrows, S. Venkatesh, S. R. Forrest, and M. E. Thompson, "High-external-quantum-efficiency organic light-emitting devices," *Opt. Lett.* **22**(6), 396–398 (1997).
11. S. Nowy, B. C. Krummacher, J. Frischeisen, N. A. Reinke, and W. Brutting, "Light extraction and optical loss mechanisms in organic light-emitting diodes: Influence of the emitter quantum efficiency," *J. Appl. Phys.* **104**(12), 123109 (2008).
12. H. Greiner, "Light extraction from organic light-emitting diode substrates: Simulation and experiment," *Jpn. J. Appl. Phys., Part 1* **46**(7A), 4125–4137 (2007).
13. M. Fujita, K. Ishihara, T. Ueno, T. Asano, S. Noda, H. Ohata, T. Tsuji, H. Nakada, and N. Shimoji, "Optical and electrical characteristics of organic light-emitting diodes with two-dimensional photonic crystals in organic/electrode layers," *Jpn. J. Appl. Phys., Part 1* **44**(6A), 3669–3677 (2005).
14. J. M. Lupton, B. J. Matterson, I. D. W. Samuel, M. J. Jory, and W. L. Barnes, "Bragg scattering from periodically microstructured light-emitting diodes," *Appl. Phys. Lett.* **77**(21), 3340–3342 (2000).
15. U. Geyer, J. Hauss, B. Riedel, S. Gleiss, U. Lemmer, and M. Gerken, "Large-scale patterning of indium tin oxide electrodes for guided mode extraction from organic light-emitting diodes," *J. Appl. Phys.* **104**(9), 093111 (2008).

16. Y. Sun and S. R. Forrest, "Enhanced light out-coupling of organic light-emitting devices using embedded low-index grids," *Nat. Photonics* **2**(8), 483–487 (2008).
17. T. W. Koh, J. M. Choi, S. Lee, and S. Yoo, "Optical outcoupling enhancement in organic light-emitting diodes: Highly conductive polymer as a low-index layer on microstructured ito electrodes," *Adv. Mater.* **22**(16), 1849–1853 (2010).
18. A. Gombert, B. Blasi, C. Buhler, P. Nitz, J. Mick, W. Hossfeld, and M. Niggemann, "Some application cases and related manufacturing techniques for optically functional microstructures on large areas," *Opt. Eng.* **43**(11), 2525–2533 (2004).
19. A. Taflove and S. C. Hagness, *Computational Electromagnetics: The Finite-Difference Time-Domain Method*, 3rd ed., Artech House, Boston (2005).